Research

Author for correspondence:
John S. Wettlaufer
e-mail: john.wettlaufer@yale.edu

Fluctuations in Arctic sea-ice extent: comparing observations and climate models

Sahil Agarwal[1] and John S. Wettlaufer[1,2,3]

[1]Yale University, New Haven, CT, USA
[2]Mathematical Institute, University of Oxford, Oxford, UK
[3]Nordita, Royal Institute of Technology and Stockholm University, Stockholm, Sweden

JSW, 0000-0002-1676-9645

The fluctuation statistics of the observed sea-ice extent during the satellite era are compared with model output from CMIP5 models using a multifractal time series method. The two robust features of the observations are that on annual to biannual time scales the ice extent exhibits white noise structure, and there is a decadal scale trend associated with the decay of the ice cover. It is shown that (i) there is a large inter-model variability in the time scales extracted from the models, (ii) none of the models exhibits the decadal time scales found in the satellite observations, (iii) five of the 21 models examined exhibit the observed white noise structure, and (iv) the multi-model ensemble mean exhibits neither the observed white noise structure nor the observed decadal trend. It is proposed that the observed fluctuation statistics produced by this method serve as an appropriate test bed for modelling studies.

This article is part of the theme issue 'Modelling of sea-ice phenomena'.

1. Introduction

Polar amplification and the ice–albedo feedback focus scientific study on the fluctuations in the areal coverage of high latitude ice. By area, on average the Southern Hemisphere ice cover is dominated by the Antarctic ice sheet, whereas in the Northern Hemisphere, the

Arctic sea-ice cover dominates. Although we can observe the daily ice cover from space, the substantial changes in Arctic ice mass during recent decades are associated with an ostensibly unmeasurable (approx. $1\,\mathrm{W\,m^{-2}}$) contribution to the surface energy balance [1]. Hence, given this sensitivity, developing a quantitative understanding of the fluctuations in sea-ice cover is important. According to the Inter-governmental Panel on Climate Change (IPCC) Fifth Assessment Report [2], the most reliably measured characteristic of sea ice is the hemispheric sea-ice extent, to which models are tuned and parametrizations refined. To this end, we compare the statistical structure of satellite observations of ice extent to that from model output.

The global climate models (GCMs) from the IPCC Assessment Report 5 (AR5) project the Arctic to be ice-free by the middle of this century, whereas the previous assessment projected this to occur at the end of the century. The AR5 models project the Arctic to be ice-free as early as 2030 to as late as 2100 ([3], fig. 1 in [4]). The high inter-model variability and the parametrization schemes and tuning used (e.g. the sea-ice albedo, clouds, convective processes) [5–9] constitute key aspects of their veracity at projecting the state of the ice cover.

To quantify the fluctuations in the ice cover from days to decades we have analysed satellite passive microwave data using a multifractal methodology [10]. We studied the Arctic equivalent sea-ice extent (EIE), where the EIE is defined as the total surface area, including land, north of the zonal-mean ice edge latitude and thus is proportional to the sine of the ice edge latitude [11]. (By studying the EIE one minimizes coastal effects.) We find that the EIE is a multifractal in time [10] and thus cannot be explained as an auto-regressive process with a single time scale (a so-called AR-1 process), as is commonly used to characterize Arctic sea ice in GCMs [12–14]. An AR-1 process is inappropriate because (i) the existence of multiple time scales in the data cannot be treated in a quantitatively consistent manner with a single decay autocorrelation. (ii) The strength of the seasonal cycle is such that, if not appropriately removed, retrievals will always produce a single characteristic time of about a year; a time scale at which all moments converge. Hence, the upper bound on the persistence time in any study that assumes an AR-1 process will inevitably be approximately 1 year, as is indeed found for ice area [13,14]. Separate studies with GCMs [15–19] also show that an upper bound exists on the predictability for the Arctic sea-ice cover and that predictability is *skilful* only on the seasonal time scales. Therefore, our approach highlights the dangers of not carefully detrending the seasonality.

2. Methods and data

In an effort to improve understanding of Arctic sea-ice behaviour in the AR5 GCMs, we compare the daily satellite observations from 1978–2005 to the model output data with daily frequency for the same period. For parity in this comparison, we analyse the 21 AR5 models (shown in table 1) with daily data in their historical runs, and use the first ensemble member from 11 of these and two from the remaining 10 models. To be consistent in our comparison of all the models and the satellite observations, a common latitude–longitude grid of $0.5° \times 0.5°$ is used and we interpolate the sea-ice concentration (or sea-ice area fraction) from the original model/observation grid onto this common grid. As is done for the observations, the sea-ice extent obtained from the models is then converted to EIE.

Next, we remove the mean seasonal cycle (the mean EIE on each calendar day of the year) from the model output. Figures 1 and 2 show the mean seasonal cycle for the Arctic sea-ice extent and the EIE for both the AR5 models and the observations. The inter-model variability is remarkable. It is noted in the IPCC report *Evaluation of climate models* [2] that models are tuned to match the observed climate system, which in turn helps to give skilful predictions. However, as is evident in figure 2, where although the models may be tuned to match the Arctic sea-ice extent (figure 1), if one calculates the EIE from the model output the variation from the observed seasonal cycle is substantial, not only in the magnitude of the mean seasonal cycle, but also in the qualitative shape of the curves. Namely, some models have a *cycloidal structure*, with a plateau shaped region in winter and a deep well structure in summer. We emphasize again that the EIE not

Table 1. Global climate models (GCMs) used in this study. Models with daily output for sea-ice extent in their historical run have been included.

institution	model name
Beijing Climate Center (BCC)	BCC_CSM1.1 (BCC Climate System Model, v. 1.1)
Centro Euro-Mediterraneo per I Cambiamenti Climatici	CMCC-CESM
Centro Euro-Mediterraneo per I Cambiamenti Climatici	CMCC-CM
Centro Euro-Mediterraneo per I Cambiamenti Climatici	CMCC-CMS
Centre National de Recherches Meteorologiques	CNRM-CM5 (Coupled Global Climate Model, v. 5)[a]
Sate Key Laboratory of Numerical Modeling for Atmospheric Sciences and Geophysical Fluid Dynamics, Institute of Atmospheric Physics	FGOALS-g2 (Flexible Global Ocean-Atmosphere-Land System Model gridpoint, v. 2)
Atmosphere and Ocean Research Institute, University of Tokyo	MIROC-ESM[a]
Atmosphere and Ocean Research Institute, University of Tokyo	MIROC-ESM-CHEM
Atmosphere and Ocean Research Institute, University of Tokyo	MIROC 4 h[a]
Atmosphere and Ocean Research Institute, University of Tokyo	MIROC version 5 (MIROC5)[a]
Met Office Hadley Centre	HadGEM2-CC (Hadley Global Environment Model 2—Carbon Cycle)[a]
Met Office Hadley Centre	HadGEM2-ES (Hadley Global Environment Model 2—Earth System)
Max Planck Institute for Meteorology (MPI-M)	MPI-ESM-LR (MPI Earth System Model, Low Resolution)[a]
Max Planck Institute for Meteorology (MPI-M)	MPI-ESM-MR (MPI Earth System Model, Medium Resolution)[a]
Max Planck Institute for Meteorology (MPI-M)	MPI-ESM-P (MPI Earth System Model, Paleo)[a]
Meteorological Research Institute (MRI)	MRI-CGCM3 (MRI Coupled Atmosphere-Ocean General Circulation Model, v. 3)
Meteorological Research Institute (MRI)	MRI-ESM1 (MRI Earth System Model, v. 1)
Norwegian Climate Centre	NorESM1-M (Norwegian Earth System Model, version 1, Medium resolution)[a]
Geophysical Fluid Dynamics Laboratory	GFDL CM3 (GFDL Climate Model, v. 3)[a]
Geophysical Fluid Dynamics Laboratory	GFDL ESM2G (GFDL Earth System Model)
Geophysical Fluid Dynamics Laboratory	GFDL ESM2M (GFDL Earth System Model)

[a]Models with two ensemble members included.

only mitigates the effects of land on the ice extent, but it also appropriately characterizes regional sea-ice characteristics. Thus, even if a model is able to faithfully reproduce the total ice extent, it is possible that regional differences between the models and the observations are large and summing these acts to minimize these differences [20], thereby leading to specious conclusions.

When viewing a time series as a temporal multifractal, there is no constraint on the number of allowable time scales present within the data. Thus, depending on the temporal resolution of the time series, one can extract all time scales corresponding to the physical processes governing the system. Kantelhardt *et al.* [21] developed a multifractal generalization of detrended fluctuation analysis (a modification of the rescaled range method used by Hurst [22] to study the dynamics of river discharge) called multifractal detrended fluctuation analysis (MF-DFA). We use a new
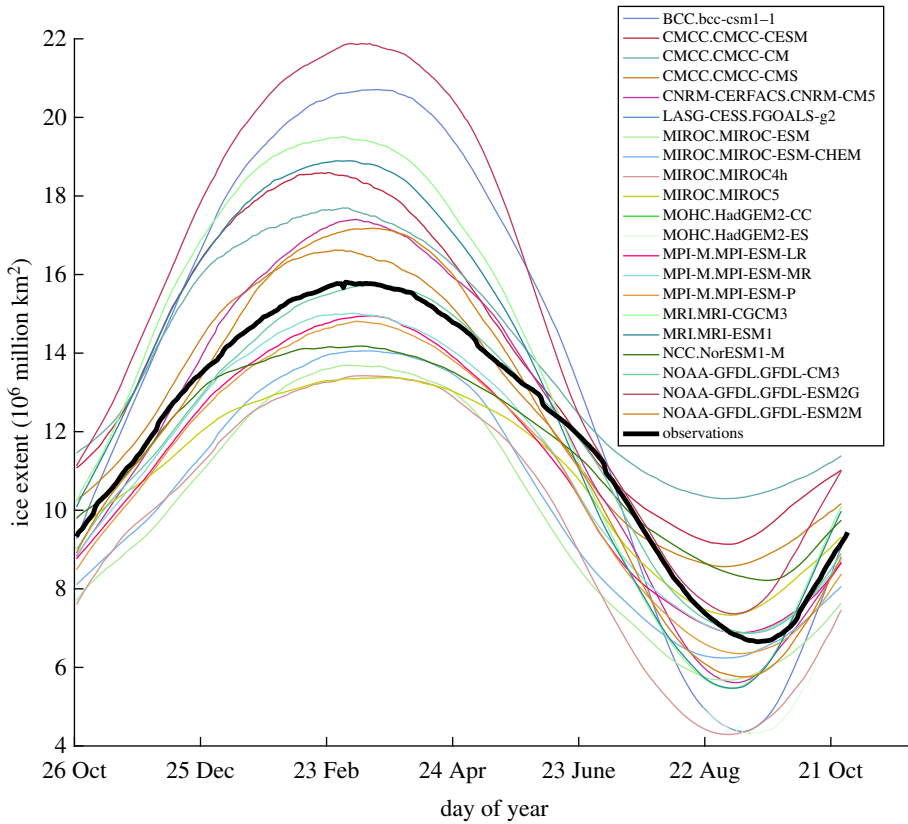
Figure 1. The mean seasonal cycle of the ice extent from the CMIP5 models is compared to the observations (in bold).

variant of MF-DFA called multifractal temporally weighted detrended fluctuation analysis (MF-TW-DFA), which exploits the intuition that points closer in time are more likely to be related than points distant in time, providing a clearer signature of long time scales present in a time series [23]. The detailed algorithm for MF-TW-DFA can be found in ([10,24,25] and references therein) and this is the approach we use to analyse and compare the EIE (without a seasonal cycle) from AR5 models to that from the satellite observations. Because of the fact that there are no *a priori* assumptions made regarding the physical processes in the system, this method has also been used to explain the dynamics of Arctic sea-ice velocity fields [24], and to detect exoplanets [25] and their atmospheres [26]. We note again that when the seasonal cycle is not removed from the sea-ice data multifractality is inhibited and hence all the time scales longer than annual are masked, which leads to erroneous interpretation of data or model output as obeying an AR-1 process.

The fluctuations in a time series are quantified with respect to a smooth *profile*, defined as the cumulative sum produced by time-weighting the data. These fluctuations are then combined to construct the fluctuation function, $F_q(s)$, for each time scale, s, under examination, where q denotes the qth moment of this function. For a given moment, the key behaviour examined is the s-dependence of $F_q(s)$, which is characterized by a generalized Hurst exponent $h(q)$, namely

$$F_q(s) \propto s^{h(q)}. \tag{2.1}$$

For example, in a monofractal time series $h(q)$ is independent of q, and thus equivalent to the classical Hurst exponent H. The exponent $h(2)$ is related to the decay of the power spectrum, $S(f)$. Hence, if $S(f) \propto f^{-\beta}$, with frequency f, then $h(2) = (1 + \beta)/2$ (e.g. [27]). Thus, for white noise $\beta = 0$, which gives $h(2) = \frac{1}{2}$, whereas for red noise $\beta = 2$, giving $h(2) = \frac{3}{2}$. Therefore, the dominant
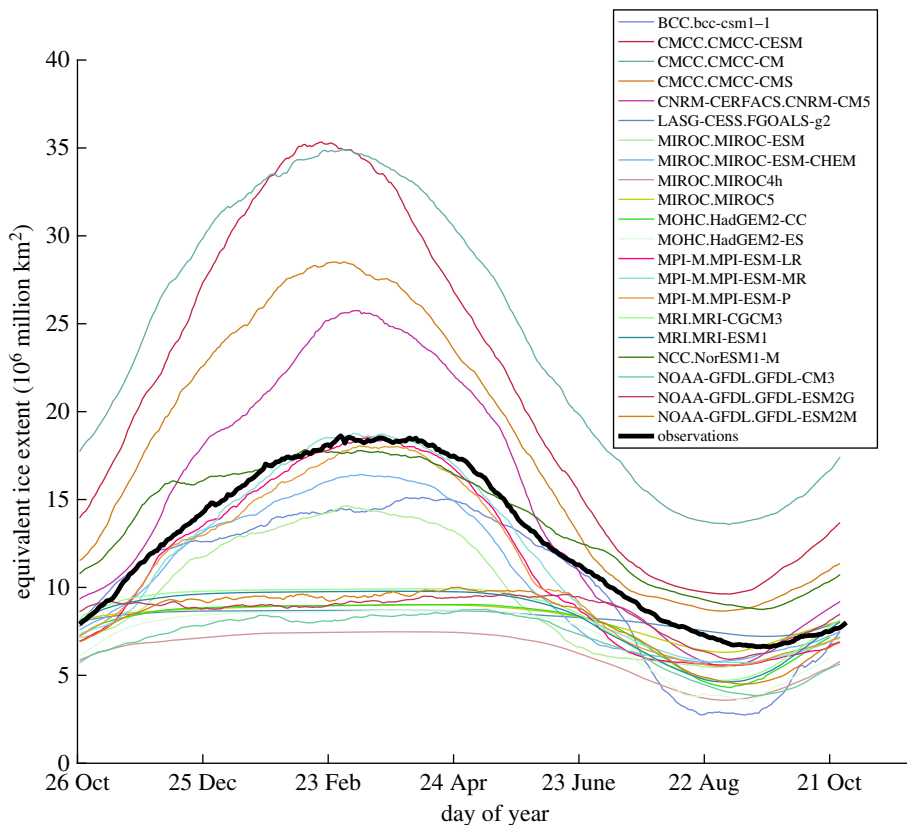
Figure 2. The mean seasonal cycle of the equivalent ice extent from the CMIP5 models is compared to the observations (in bold).

time scales found using MF-TW-DFA also capture the corresponding temporal dynamics, such as white noise, red noise and correlation structure, which allows us to construct stochastic models for the observed processes, such as the statistical structure and dynamics of sea-ice velocity fields [24]. The 'crossover' or 'dominant' time scale is defined as that at which the fluctuation function $\log_{10} F_2(s)$ changes slope with respect to $\log_{10} s$. These occur when slope of the curve exceeds a threshold of $C_{th} = 0.01$.

3. Discussion

Here we compare the fluctuation functions from the AR5 models to the observations. The nature and number of figures are such that the majority of the results are presented in appendix A, and here we summarize the key features, which are (i) large inter-model variability in the crossover time scales extracted from the models, (ii) none of the models exhibit the decadal time scales found in the satellite observations, and (iii) only five (CNRM-CM5, MRI-CGCM3 , MRI-ESM1, FGOALS-g2, MIROC5 (second ensemble member)) of the 21 models exhibit the white noise structure (shown in figure 3) observed in the satellite record on annual to biannual time scales. Additionally, only four models exhibit time scales approaching decadal (7.2 years in BCC1-1, 4.8 years in FGOALS-g2, 7.9 years in NorESM1, 4.5 years in the second ensemble member of NorESM1 and 6 years in GFDL-ESM2G), whereas in all of the other models the longest time scale is of the order a year.

The high-frequency processes governing shorter time scales are associated with the influence of synoptic systems, the intermediate time scales are seasonal and the longer—decadal—time scales are generally ascribed to climate processes [10]. For example, Agarwal & Wettlaufer [24]
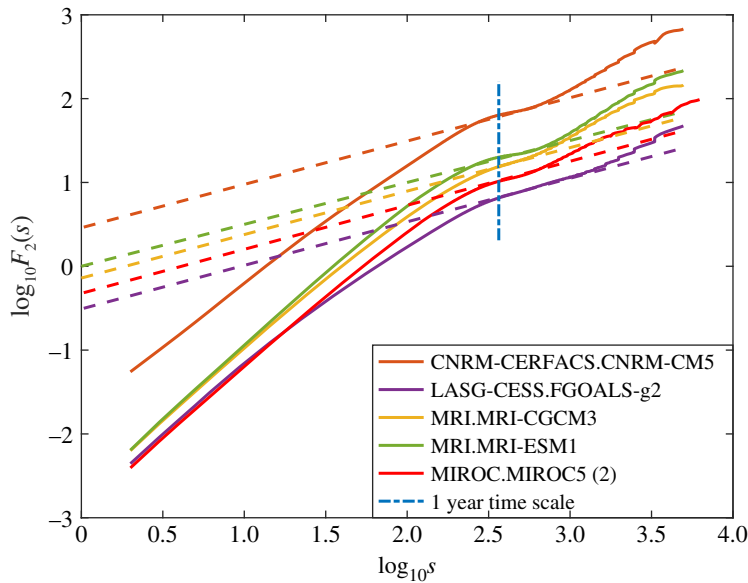
Figure 3. For $q = 2$, the fluctuation function for EIE for the five (of the 21 examined) GCMs that exhibit the white noise structure observed in the satellite data labelled in the inset. The slanted straight dashed lines denote white noise with $h(2) = \frac{1}{2}$, the vertical line denotes 1 year. The time range is 1 day $\leq s \leq$ 13.6 years.
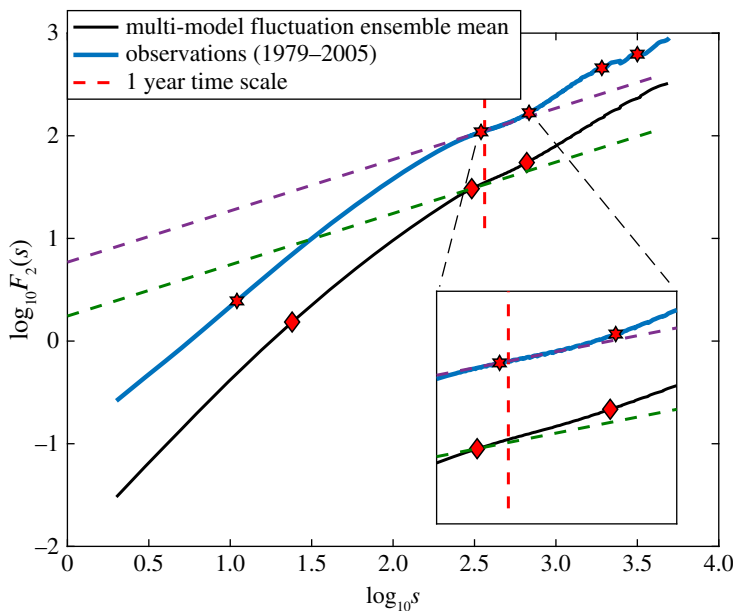

Figure 4. For $q = 2$, the fluctuation functions for EIE from the multi-model ensemble mean (black) and the satellite observations (blue). The slanted straight dashed lines denote white noise with $h(2) = \frac{1}{2}$, the vertical line denotes 1 year. The time range is 1 day $\leq s \leq$ 13.6 years. Diamonds denote crossover time scales for the MMEM (24 days, 304 days and 658 days), and hexagrams denote crossover time scales for the satellite observations (11 days, 347 days, 684 days, 5.2 years and 8.6 years).

demonstrated that on annual–biannual time scales, the sea-ice extent is largely controlled by the wind fields over the Arctic. By comparing the sea-ice volumes from the models with the PIOMAS [28] dataset, Shu *et al.* [29] showed that the sea-ice thickness produced in the CMIP5 models is much less than what is observed. Therefore, although analysis of the Arctic sea-ice velocity fields from the CMIP5 models shows that most models reproduce the statistical

characteristics of the observed velocity fields, if the sea ice produced by the models is too thin, the spectrum of its response to wind forcing will change. For example, Colony & Thorndike [30] showed that local low-frequency ice motion is linearly correlated with local synoptic wind forcing, but the local inertial motion is not, despite a high coherency between the inertial motion of the ice on the same length (approx. 100 km) scales. This highlights the role of mechanical interactions between ice floes on short time scales, which would not be captured in models producing thinner ice.

Wang & Overland [4] analysed the sea-ice extent in the CMIP5 models and concluded that the Arctic would be ice-free in the next 14–36 years with a median of 28 years, based on the model spread. Massonnet *et al.* [31] tried to reduce the CMIP5 uncertainty for the Arctic to become ice-free, finding a spread of about 40–60 years. However, the absence of the longer time scales in the models that we have shown here provides a challenge for their predictive capability on decadal time scales. The origin of this lack of parity between satellite observations and the models will of course differ from model to model, but should provide an observational and statistical constraint for model physics, which has evidently not been met by the tuning and parametrization schema used thus far. Indeed, Swart *et al.* [32] showed how a deliberately-biased picking of short-term trends to predict the long-term behaviour of sea-ice extent can lead to false conclusions. Similarly, our study demonstrates both quantitatively and qualitatively the reason behind such high inter-model spread on decadal time scales and longer.

4. Conclusion

The observed Arctic sea-ice extent can be thought of as the 'output' of the highly complex nonlinear interactions governing the air/sea/ice system. It is a central goal of modelling to try and reproduce this output. A model can be tuned to match some of the observations, but if one is interested in making predictions about the future state of the system, one seeks to know the key underlying physical and dynamical processes and how they govern its central statistical response. Many studies compare the multi-model ensemble mean (MMEM) to observations, and argue that a sufficient condition for predictability is that the observations are within 1 s.d. of the MMEM. However, here we find that even the MMEM does not exhibit the robust observational features of white noise characteristics on annual–biannual time scales or the characteristic decadal time scales. Figure 4 compares the fluctuation functions for the EIE from the satellite observations (blue) to the MMEM. The longest crossover time scale present in the MMEM data is 1.8 years and that from the observations is 8.6 years. Therefore, simply summing different models to produce the MMEM does not provide the observed statistical structure of the ice pack.

A central role of observations is to produce robust statistical metrics that can serve as a target for modelling. Whereas, even with incorrect physics, it is possible to match features of the observations, capturing the appropriate statistical properties should provide important litmus tests for models. Our method is agnostic with regard to the number of crossover time scales, and hence associated processes, that may be present in the system. Therefore, we hope that the fact that we capture both the shortest and longest observed processes in the ice pack will provide a useful and robust test bed for modelling studies.

Appendix A

Below we provide additional figures 5–8 of the fluctuation functions, $F_q(s)$, versus time scale, s, for the CMIP5 models labelled therein and described in table 1. Changes in the slope of $F_q(s)$ occur at
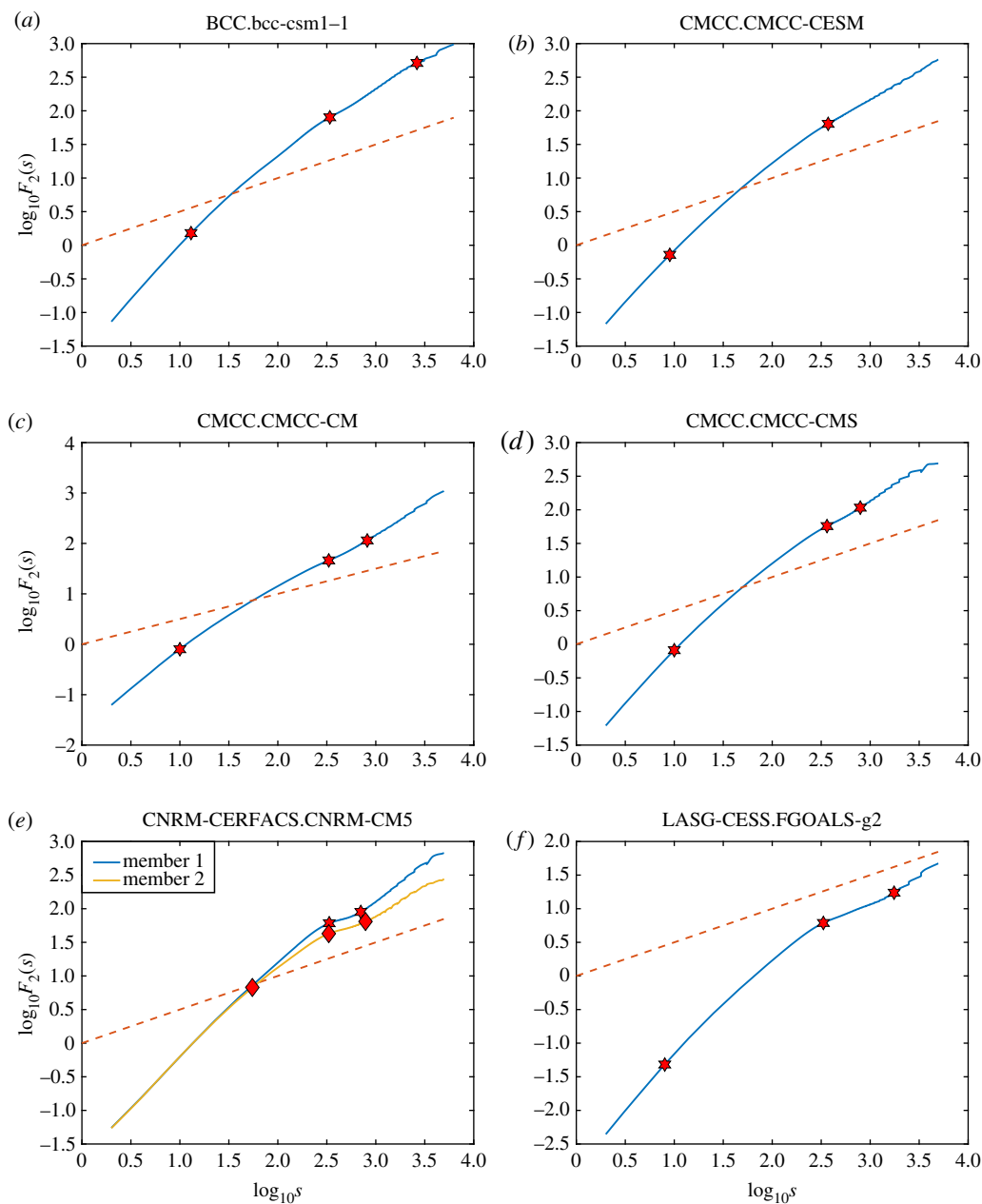
Figure 5. Fluctuation functions (solid) for CMIP5 AR5 models. The respective crossover time scales present are (*a*) 13 days, 340 days, 7.2 years (stars);(*b*) 9 days, 372 days (stars); (*c*) 10 days, 331 days, 818 days (stars); (*d*) 10 days, 359 days, 793 days (stars); (*e*) member 1: 335 days, 703 days (stars); member 2: 55 days, 331 days, 785 days (diamonds); (*f*) 8 days, 333 days, 4.8 years (stars). The dashed line (orange) denotes a slope of $\frac{1}{2}$. (Online version in colour.)

the particular crossover time scales denoted in the caption. The main text describes the dynamics associated with these time scales.
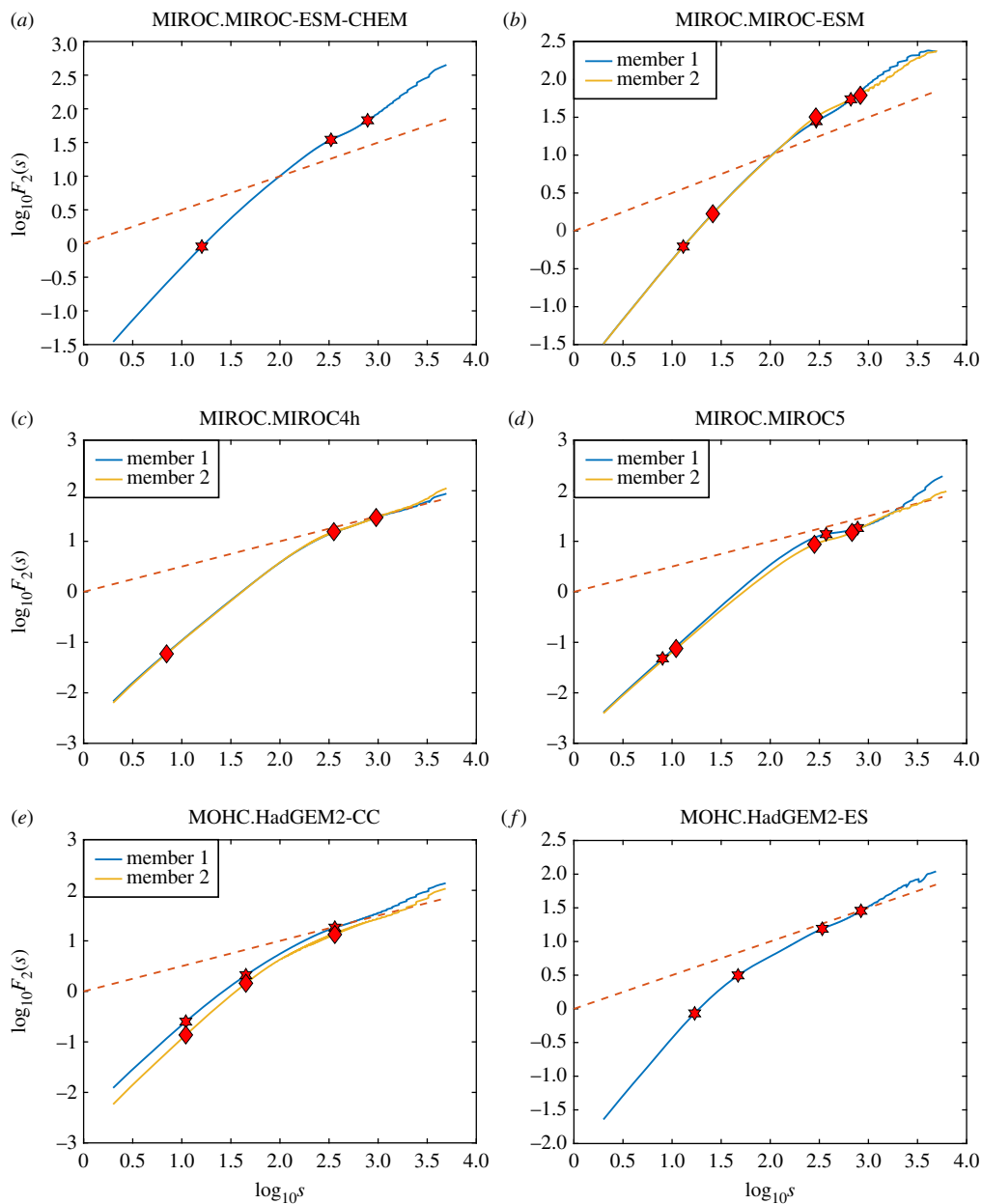
8

rsta.royalsocietypublishing.org *Phil. Trans. R. Soc. A* **376**: 20170332

Figure 6. Fluctuation functions (solid) for CMIP5 AR5 models. The respective crossover time scales present are (*a*) 16 days, 330 days, 782 days (stars); (*b*) member 1: 13 days, 294 days, 661 days (stars); member 2: 26 days, 292 days, 828 days (diamonds); (*c*) member 1: 7 days, 354 days, 955 days (stars); member 2: 7 days, 354 days, 955 days (diamonds); (*d*) member 1: 8 days, 371 days, 777 days (stars); member 2: 11 days, 282 days, 681 days (diamonds); (*e*) member 1: 11 days, 45 days, 362 days (stars); member 2: 11 days, 45 days, 362 days (diamonds); (*f*) 17 days, 47 days, 339 days, 840 days (stars). The dashed line (orange) denotes a slope of $\frac{1}{2}$. (Online version in colour.)
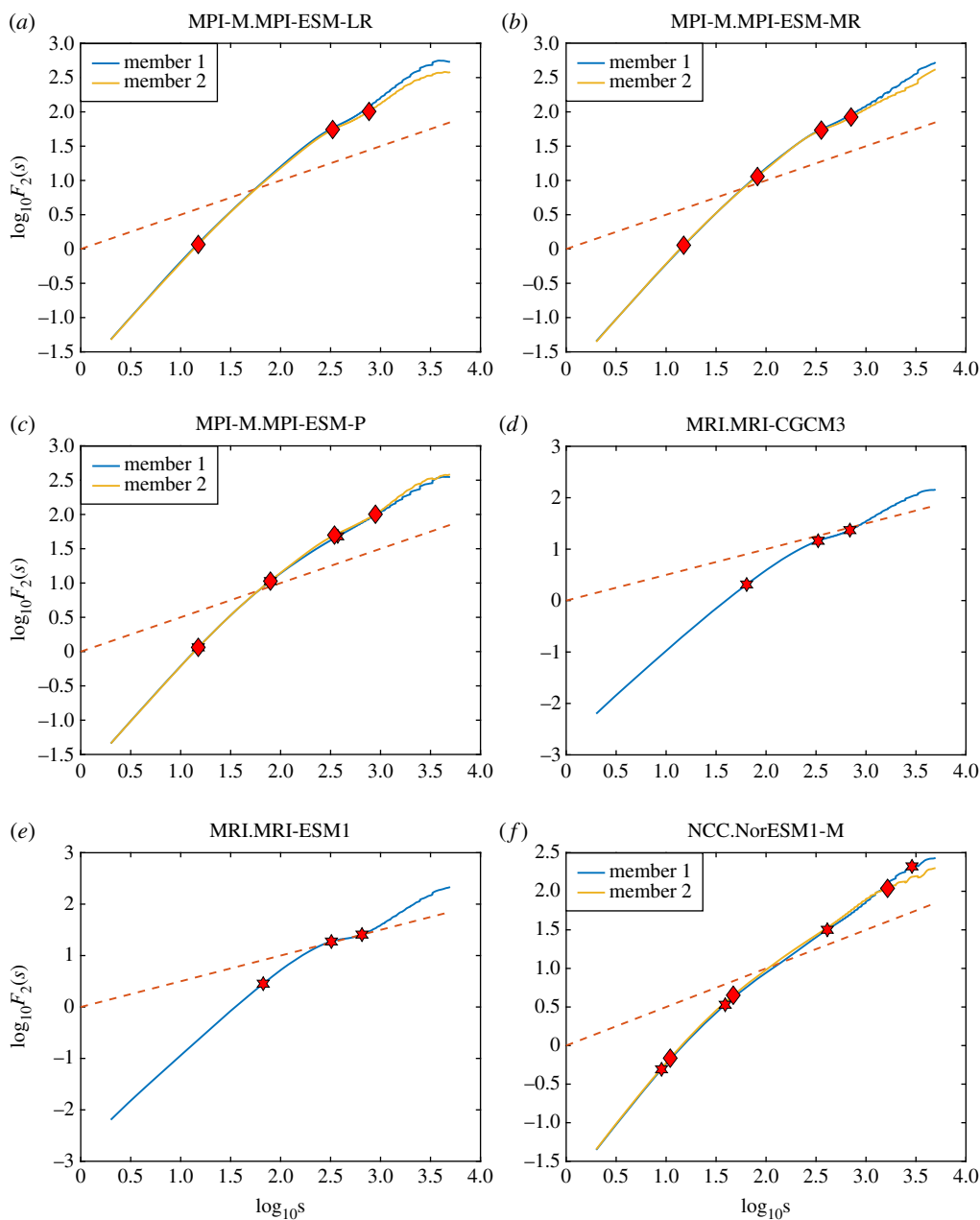
Figure 7. Fluctuation functions (solid) for CMIP5 AR5 models. The respective crossover time scales present are (*a*) member 1: 15 days, 328 days, 760 days (stars); member 2: 15 days, 332 days, 768 days (diamonds); (*b*) member 1: 15 days, 82 days, 357 days, 708 days (stars); member 2: 15 days, 82 days, 357 days, 710 days (diamonds); (*c*) member 1: 15 days, 79 days, 373 days (stars); member 2: 15 days, 79 days, 346 days, 889 days (diamonds); (*d*) 64 days, 332 days, 690 days (stars); (*e*) 67 days, 322 days, 652 days (stars); (*f*) member 1: 9 days, 39 days, 410 days, 7.9 years (stars); member 2: 11 days, 47 days, 4.5 years (diamonds). The dashed line (orange) denotes a slope of $\frac{1}{2}$. (Online version in colour.)
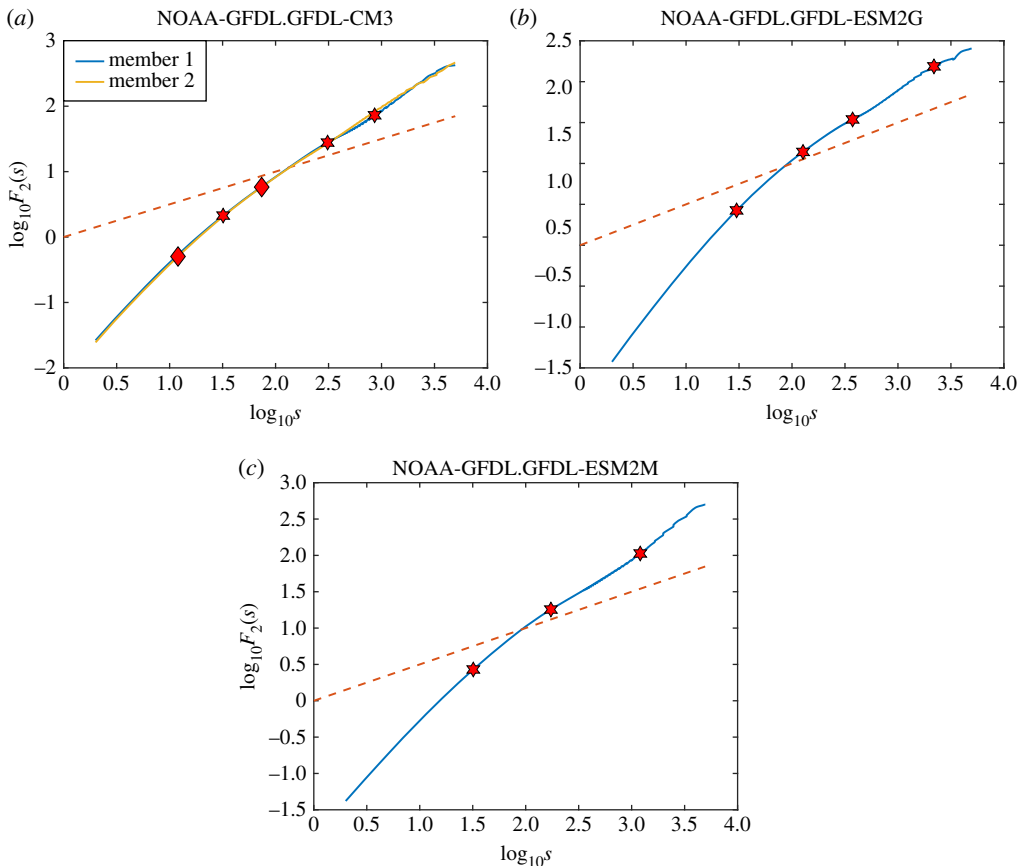
Figure 8. Fluctuation functions (solid) for CMIP5 AR5 models. The respective crossover time scales present are (*a*) member 1: 32 days, 310 days, 861 days (stars); member 2: 12 days, 74 days (diamonds); (*b*) 30 days, 127 days, 373 days, 6 years (stars); (*c*) 32 days, 173 days, 3.3 years (stars). The dashed line (orange) denotes a slope of $\frac{1}{2}$. (Online version in colour.)

References

1. Kwok R, Untersteiner N. 2011 The thinning of Arctic sea ice. *Phys. Today* **64**, 36–41. (doi:10.1063/1.3580491)
2. IPCC. 2013 *Evaluation of climate models*, pp. 741–866. Cambridge, UK: Cambridge University Press,
3. Stroeve JC, Kattsov V, Barrett A, Serreze M, Pavlova T, Holland M, Meier WN. 2012 Trends in Arctic sea ice extent from CMIP5, CMIP3 and observations. *Geophys. Res. Lett.* **39**, L16502. (doi:10.1029/2012gl052676)
4. Wang M, Overland JE. 2012 A sea ice free summer Arctic within 30 years: an update from CMIP5 models. *Geophys. Res. Lett.* **39**, L18501. (doi:10.1029/2012gl052868)
5. Eisenman I, Untersteiner N, Wettlaufer JS. 2007 On the reliability of simulated Arctic sea ice in global climate models. *Geophys. Res. Lett.* **34**, L10501. (doi:10.1029/2007GL029914)
6. DeWeaver ET, Hunke EC, Holland MM. 2008 Comment on 'On the reliability of simulated Arctic sea ice in global climate models'. *Geophys. Res. Lett.* **35**, L04501. (doi:10.1029/2007gl031325)
7. Eisenman I, Untersteiner N, Wettlaufer JS. 2008 Reply to Comment by DeWeaver et al. on 'On the reliability of simulated Arctic sea ice in global climate models'. *Geophys. Res. Lett.* **35**, L04502. (doi:10.1029/2007gl032173)
8. Mauritsen T *et al.* 2012 Tuning the climate of a global model. *J. Adv. Model. Earth Syst.* **4**, M00A01. (doi:10.1029/2012ms000154)

9. Hourdin F *et al.* 2013 LMDZ5B: the atmospheric component of the IPSL climate model with revisited parameterizations for clouds and convection. *Clim. Dyn.* **40**, 2193–2222. (doi:10.1007/s00382-012-1343-y)

10. Agarwal S, Moon W, Wettlaufer JS. 2012 Trends, noise and reentrant long-term persistence in Arctic sea ice. *Proc. R. Soc. A* **468**, 2416–2432. (doi:10.1098/rspa.2011.0728)

11. Eisenman I. 2010 Geographic muting of changes in the Arctic sea ice cover. *Geophys. Res. Lett.* **37**, L16501. (doi:10.1029/2010gl043741)

12. Piwowar JM, Wessel GR, LeDrew EF. 1996 Image time series analysis of Arctic sea ice. In *IGARSS'96. 1996 International Geoscience and Remote Sensing Symposium. 'Remote Sensing for a Sustainable Future', Lincoln, NE*, vol. 1, pp. 645–647. New York, NY: IEEE.

13. Blanchard-Wrigglesworth E, Armour KC, Bitz CM, DeWeaver E. 2010 Persistence and inherent predictability of Arctic sea ice in a GCM ensemble and observations. *J. Clim.* **24**, 231–250. (doi:10.1175/2010jcli3775.1)

14. Armour KC, Bitz CM, Thompson L, Hunke EC. 2011 Controls on Arctic sea ice from first-year and multiyear ice survivability. *J. Clim.* **24**, 2378–2390. (doi:10.1175/2010JCLI 3823.1)

15. Lindsay RW, Zhang J, Schweiger AJ, Steele MA. 2008 Seasonal predictions of ice extent in the Arctic Ocean. *J. Geophys. Res. Oceans* **113**, C02023. (doi:10.1029/2007jc004259)

16. Wang W, Chen M, Kumar A. 2012 Seasonal prediction of Arctic sea ice extent from a coupled dynamical forecast system. *Mon. Weather Rev.* **141**, 1375–1394. (doi:10.1175/mwr-d-12-00057.1)

17. Chevallier M, Salas y Mélia D, Voldoire A, Déqué M, Garric G. 2013 Seasonal forecasts of the pan-Arctic sea ice extent using a GCM-based seasonal prediction system. *J. Clim.* **26**, 6092–6104. (doi:10.1175/JCLI-D-12-00612.1)

18. Sigmond M, Fyfe JC, Flato GM, Kharin VV, Merryfield WJ. 2013 Seasonal forecast skill of Arctic sea ice area in a dynamical forecast system. *Geophys. Res. Lett.* **40**, 529–534. (doi:10.1002/grl.50129)

19. Tietsche S, Day JJ, Guemas V, Hurlin WJ, Keeley SPE, Matei D, Msadek R, Collins M, Hawkins E. 2014 Seasonal to interannual Arctic sea ice predictability in current global climate models. *Geophys. Res. Lett.* **41**, 1035–1043. (doi:10.1002/2013GL058755)

20. Li D, Zhang R, Knutson TR. 2017 On the discrepancy between observed and CMIP5 multi-model simulated Barents Sea winter sea ice decline. *Nat. Commun.* **8**, 14991. (doi:10.1038/ncomms14991)

21. Kantelhardt JW, Zschiegner SA, Koscielny-Bunde E, Havlin S, Bunde A, Stanley HE. 2002 Multifractal detrended fluctuation analysis of nonstationary time series. *Physica A* **316**, 87–114. (doi:10.1016/s0378-4371(02)01383-3)

22. Hurst HE. 1951 Long-term storage capacity of reservoirs. *Trans. Am. Soc. Civil Eng.* **116**, 770–808.

23. Zhou Y, Leung Y. 2010 Multifractal temporally weighted detrended fluctuation analysis and its application in the analysis of scaling behavior in temperature series. *J. Stat. Mech. Theor. Exp.* **2010**, P06021. (doi:10.1088/1742-5468/2010/06/p06021)

24. Agarwal S, Wettlaufer JS. 2017 The statistical properties of sea ice velocity fields. *J. Clim.* **30**, 4873–4881. (doi:10.1175/JCLI-D-16-0653.1)

25. Agarwal S, Sordo FD, Wettlaufer JS. 2017 Exoplanetary detection by multifractal spectral analysis. *Astron. J.* **153**, 12. (doi:10.3847/1538-3881/153/1/12)

26. Agarwal S, Wettlaufer JS. 2017 Exoplanet atmosphere retrieval using multifractal analysis of secondary eclipse spectra. (http://arxiv.org/abs/1710.09870).

27. Rangarajan G, Ding M. 2000 Integrated approach to the assessment of long range correlation in time series data. *Phys. Rev. E* **61**, 4991–5001. (doi:10.1103/PhysRevE.61.4991)

28. Zhang J, Rothrock DA. 2003 Modeling global sea ice with a thickness and enthalpy distribution model in generalized curvilinear coordinates. *Mon. Weather Rev.* **131**, 845–861. (doi:10.1175/1520-0493(2003)131<0845:MGSIWA>2.0.CO;2)

29. Shu Q, Song Z, Qiao F. 2015 Assessment of sea ice simulations in the CMIP5 models. *Cryosphere* **9**, 399–409. (doi:10.5194/tc-9-399-2015)

30. Colony R, Thorndike AS. 1980 The horizontal coherency of the motion of summer Arctic sea ice. *J. Phys. Ocean.* **10**, 1281–1289. (doi:10.1175/1520-0485(1980)010<1281:THCOTM>2.0.CO;2)

31. Massonnet F, Fichefet T, Goosse H, Bitz CM, Philippon-Berthier G, Holland MM, Barriat PY. 2012 Constraining projections of summer Arctic sea ice. *Cryosphere* **6**, 1383–1394. (doi:10.5194/tc-6-1383-2012)
32. Swart NC, Fyfe JC, Hawkins E, Kay JE, Jahn A. 2015 Influence of internal variability on Arctic sea-ice trends. *Nat. Clim. Change* **5**, 86–89. (doi:10.1038/nclimate2483)

13

rsta.royalsocietypublishing.org *Phil. Trans. R. Soc. A* **376**: 20170332